JCIM JOURNAL OF CHEMICAL INFORMATION AND MODELING

pubs.acs.org/jcim Article

# SINAPs: A Software Tool for Analysis and Visualization of Interaction Networks of Molecular Dynamics Simulations

Corentin Bedart,* Nicolas Renault, Philippe Chavatte, Adeline Porcherie, Abderrahim Lachgar, Monique Capron, and Amaury Farce*

Cite This: J. Chem. Inf. Model. 2022, 62, 1425−1436 Read Online

ACCESS | Metrics & More | Article Recommendations | Supporting Information

**ABSTRACT:** As long as the structural study of molecular mechanisms requires multiple molecular dynamics reflecting contrasted bioactive states, the subsequent analysis of molecular interaction networks remains a bottleneck to be fairly treated and requires a user-friendly 3D view of key interactions. Structural Interaction Network Analysis Protocols (SINAPs) is a proprietary python tool developed to (i) quickly solve key interactions able to distinguish two protein states, either from two sets of molecular dynamics simulations or from two crystallographic structures, and (ii) render a user-friendly 3D view of these key interactions through a plugin of UCSF Chimera, one of the most popular open-source viewing software for biomolecular systems. Through two case studies, glucose transporter-1 (GLUT-1) and A2A adenosine receptor (A2AR), SINAPs easily pinpointed key interactions observed experimentally and relevant for their bioactivities. This very effective tool was thus applied to identify the amino acids involved in the molecular enzymatic mechanisms ruling the activation of an immunomodulator drug candidate, P28 glutathione-S-transferase (P28GST). SINAPs is freely available at https://github.com/ParImmune/SINAPs.

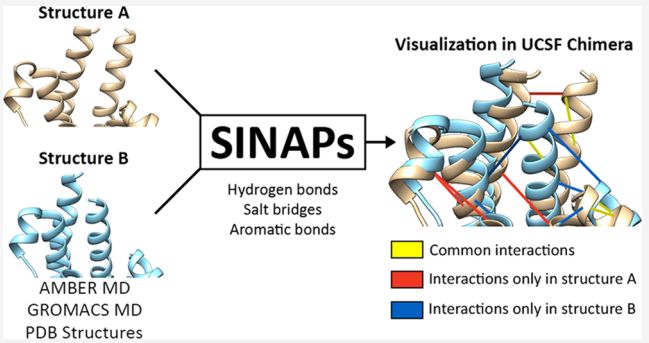


## INTRODUCTION

Molecular dynamics (MD) simulations are advanced methods for studying the evolution of a system of particles over time. Applied to biological macromolecules, these methods allow the study of their functional mechanism, the binding kinetics of molecular modulators such as small organic or macromolecular partners, as well as the identification of new druggable pockets for the discovery of new active compounds through some computational drug design processes.

The recording interval of the frames of MD simulations is a parameter that must be optimized. A too long interval can lead to missing valuable information. A too short interval will increase the quality and quantity of information generated but lead to a drastic increase of the weight of MD trajectories.[1,2] As these simulations generate a huge amount of data, the analysis phase is a bottleneck.[3,4] The use of several tools is therefore mandatory to optimize the analysis,[1] seeking, among others, to highlight differences in the interactions during the simulation.

Some tools take as input molecular dynamics trajectories and calculate the interactions but do not have an adequate display of the results. This is the case of tools proposed directly with the molecular dynamics software, such as GROMACS[5] or AMBER via cpptraj,[6,7] which propose textual results. The 3D viewer VMD[8] provides analysis of hydrogen and ionic bonds over time with the timeline utility but only gives general statistics in the form of graphs. A third-party plugin called PyContact[9] improves the flaws of VMD in the calculation of interactions but does not provide a visual representation either. RIP-MD[10] displays its results in Cytoscape[11] but loses the information of the three-dimensional structure of the protein. MDcons[12] provides intermolecular contact maps from molecular dynamics trajectories of protein complexes but does not provide information on intramolecular interactions. CONAN[13] produces contact maps along trajectories as well as visual output through the creation of heatmap images or animations but without representations of 3D structures. G_contacts[14] proposes a set-decomposition algorithm to detect all contacting atoms or residues during MD simulations, faster than traditional brute-force methods. Finally, NAPS[15] is an online web server that does not perform molecular interaction networks but centrality-based networks and thus does not take into account nonbonded interactions.

Received: July 16, 2021
Published: March 3, 2022





https://doi.org/10.1021/acs.jcim.1c00854
J. Chem. Inf. Model. 2022, 62, 1425−1436

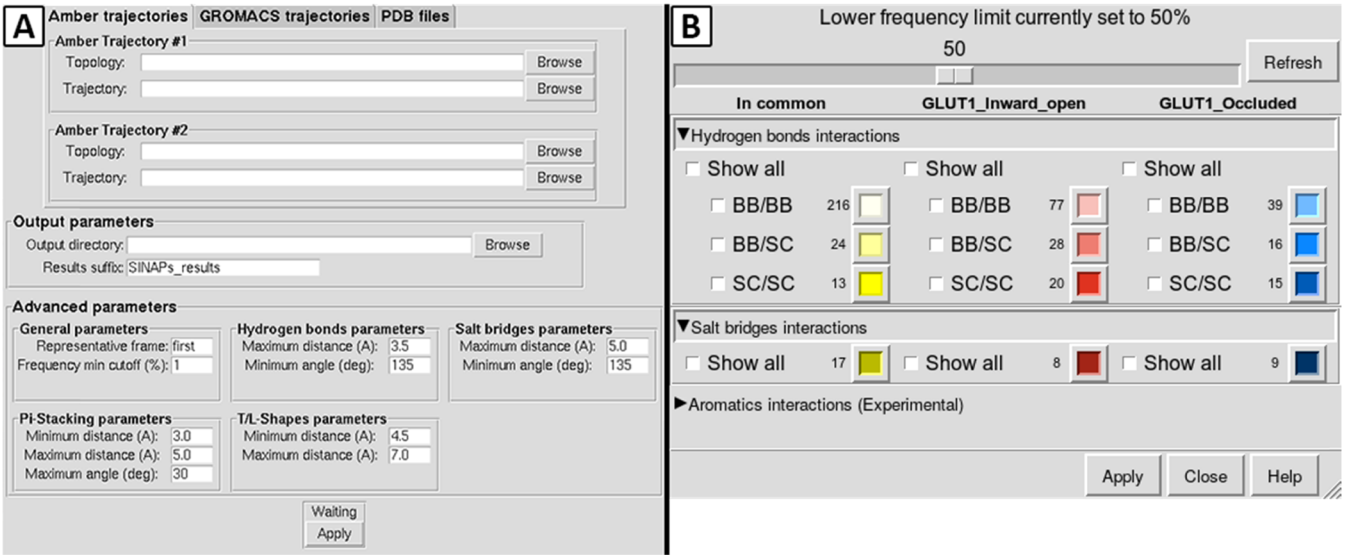


**Figure 1.** Graphical interfaces of the analysis software of SINAPs (A) and the visualization extension of SINAPs in UCSF Chimera (B). BB: backbone chain; SC: side chain; T-shape: aromatic edge-to-face interaction; L-shape: aromatic displaced edge-to-face interaction.

Other tools offer interesting graphical representations but are not adapted to molecular dynamics trajectories as they only take PDB structures as input. This is the case of the interaction calculation tools proposed by the main visualization software such as UCSF Chimera[16] or PyMOL,[17] or more specific to ligand−protein interactions such as LigPlot+.[18] In addition, some tools offer a link between Cytoscape and UCSF Chimera, such as structureViz[19] and RINspector,[20] but only perform centrality interaction networks.

Tools hosted online on web servers are generally to be avoided, as they may disappear at any time and may cause privacy issues for confidential research subjects.

There is, therefore, no perfect tool available offline that performs both analysis and visualization. The SINAPs tool presented in this paper achieves a balanced compromise. The SINAPs analyzer tool evaluates the differences in interactions between two molecular systems. Then, the SINAPs visualization tool provides a simplified visualization of the results taking into account the structural context through an extension to the UCSF Chimera visualization software.[16]

To assess its usefulness, SINAPs was applied to several case studies covering most of its applications. The first simplest case was to compare two molecular interaction networks from two crystallographic structures exhibiting contrasted bioactivities—here, the class-A A2AR GPCR complexed with agonist or antagonist ligands. The second more sophisticated case was based on the differential study of two multiconformational sets, each carried out from MD trajectories of GLUT-1. In addition, an exploratory study was performed using the classical MD of a protein drug candidate, P28GST, to assist the study of its molecular mechanism of action.

All information about SINAPs, including download information and documentation, can be found on the following website: https://github.com/ParImmune/SINAPs.

## MATERIALS AND METHODS

**Software Overview.** SINAPs includes two separate programs working together. The first component is a Python3 program analyzing the differences between two interaction networks. It takes as input two single structures (i.e., PDB crystallographic structures) with the same number of residues or two multiconformational subsets from AMBER[6] and GROMACS[5] MD trajectories (Figure 1A). A MD trajectory may be divided into several parts to study the conformational changes occurring during the simulation.

The software first extracts the two structural templates, fits them according to $\alpha$-trace, and only keeps the backbone atoms to facilitate the future visualization within UCSF Chimera.[21] Concerning the two multiconformational MD subsets, the structural templates are by default the first frame of both MD trajectories. The particularity of multiconformational analysis is based on the exhaustive exploration of interactions over all trajectory frames to calculate the frequency of nonbonded interactions formed over time while allowing precise control of the defined parameters of each type of interaction.

SINAPs' default settings have been set from the literature, but the distance and angle criteria are easily editable. Detection of hydrogen bonds is computed from a native pytraj function, search_hbonds.[7,22] This function searches for bonds by geometric criteria according to the maximum distance between the donor hydrogen and the acceptor (set at 3.5 Å), as well as the minimum angle between the donor, its hydrogen, and the acceptor (set at 135°).[23] Detection of salt bridges is computed with the same function, limiting donor residues to LYS and ARG, acceptor residues to GLU and ASP, and increasing the maximum bonding distance compared to hydrogen bonds from 3.5 to 5 Å.[23,24]

Detection of aromatic−aromatic interactions is computed from a homemade function based on geometric criteria for TYR, PHE, HIS, and TRP residues.[25,26] From the centroid and the normal vector of aromatic rings, several values are calculated: the distance between two centroids in Ångström, the planar angle describing the tilt of one aromatic ring relative to the other, and the orientation angle describing the offset of one aromatic ring relative to the other, both expressed in degrees modulo 90°.[26] Then, based on the following parameters:

- A Pi-stacking between two aromatic rings is defined if the distance between these two rings is within a defined range (set from 3 to 5 Å), if the planar angle is between 0° and


https://doi.org/10.1021/acs.jcim.1c00854
J. Chem. Inf. Model. 2022, 62, 1425−1436

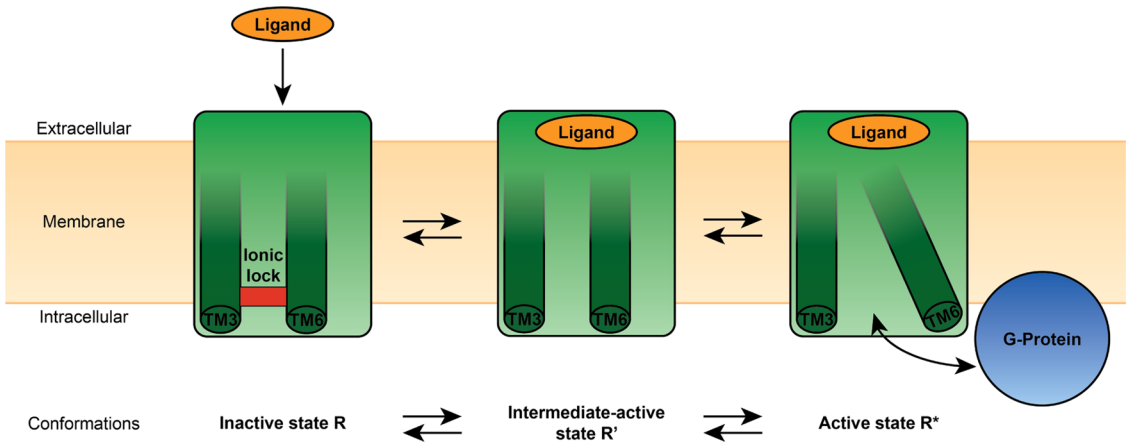


**Figure 2.** Simplified scheme of the mechanism of action of A2AR, moving from the inactive R state with the presence of the ionic lock, passing through the intermediate-active R′ state with the interaction with an activating ligand and the loss of the ionic lock, and then the active R* state with interactions with an activating ligand and a G-protein.

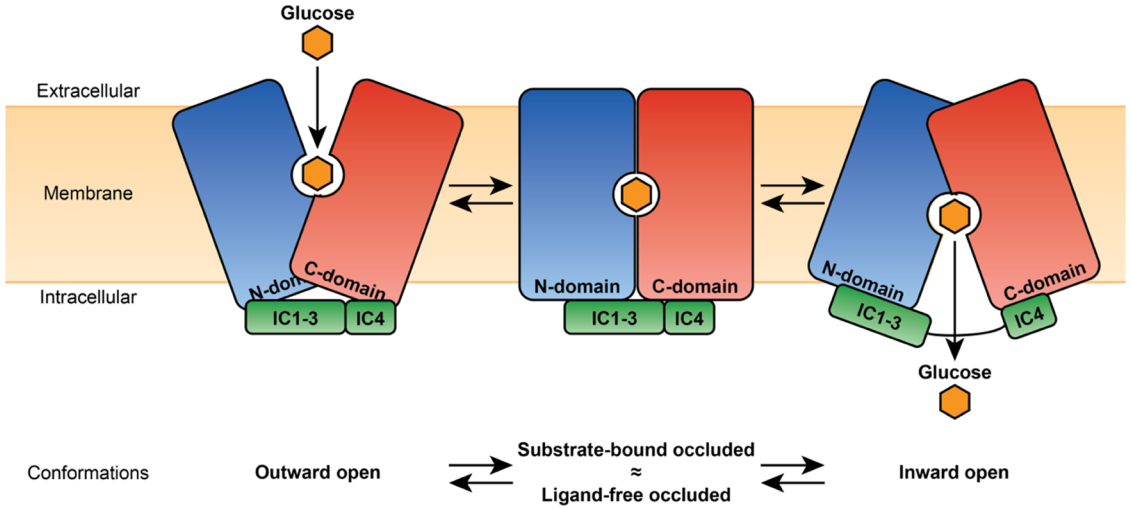


**Figure 3.** Simplified scheme of the GLUT-1 mechanism.

20° degrees, and if the orientation angle is between 0 and 30° (customizable value).

- A T-shape is defined if the distance between the two rings is within a defined range (set from 4.5 to 7 Å), if the planar angle is between 0 and 60°, and if the orientation angle is between 0 and 30° or 60 and 90°.
- An L-shape is defined if the distance between the two rings is within a defined range (set from 4.5 to 7 Å), if the planar angle is between 0 and 60°, and if the orientation angle is between 30 and 60°.

The output of the analysis tool is a list of interactions observed in the different input files, including the number of the residues involved in a given interaction, its type and frequency in each file, and the chosen representative frames extracted in the PDB format.

The second component is a Python2 add-on to USCF Chimera,[16] which allows the visualization of the results calculated by the first SINAPs Python3 tool. It takes as input the directory containing the results of the molecular interaction network analysis tool. After loading, this extension allows the observation of the representative frame of each simulation by displaying each type of nonbonded molecular interactions via a user-defined frequency lower limit and finely controlled mode of representation (Figure 1B).

**Case Studies for Depiction of Critical Interaction Networks.** *Comparison of PDB Files: Adenosine A2A Receptor.* The human adenosine A2A receptor (A2AR) belongs to the G-protein-coupled receptor superfamily, with four different ligand-bound states during its activation: two inactive R states with and without an "ionic lock" close to the cytoplasmic surface, an intermediate-active R′ state with the presence of a ligand, and a G-protein-bound R* active state[27] (Figure 2).

The study of A2AR is based on crystallographic structures of the inactive conformation bound to the inverse agonist ZM241385 (PDB ID: 3PWH),[28] the intermediate-active conformation bound to adenosine (PDB ID: 2YDO),[29] and the active conformation bound to NECA (PDB ID: 5G53).[30] Using UCSF Chimera, other cocrystallized compounds and alternate positions of several residues were removed, and the hydrogen atoms were added. To ensure that SINAPs correctly considers the input structures by having the same number of residues in each structure, the residues 8−146, 159−208, and 225−305 were kept. Finally, the prepared structures were compared using SINAPs.



https://doi.org/10.1021/acs.jcim.1c00854
J. Chem. Inf. Model. 2022, 62, 1425−1436

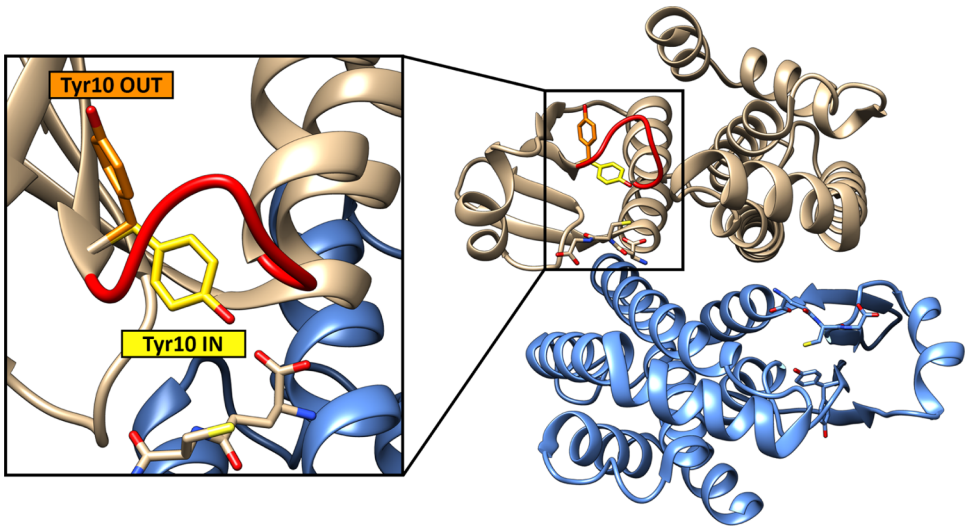


**Figure 4.** Scheme of the different conformations of Tyr10. The loop following Tyr10 is represented in red.

*Comparison of Dynamic Trajectories: Glucose Transporter-1.* Glucose transporter-1 (GLUT-1) transfers glucose across the plasma membrane of numerous cells. During glucose transport, the receptor exhibits several different structural conformations (Figure 3). In this case, we focused particularly on both closed and open-inward conformations.[31]

Before the comparative study of the multiple MD-based conformations of the GLUT-1 receptor, we prepared the starting conformations: the inward-open conformation was extracted from the crystallographic structure of the human GLUT-1 (PDB ID: 4PYP),[31] whereas the occluded conformation was built by homology modeling using target-template alignment of SWISS-MODEL,[32,33] starting from the human canonical amino acid sequence and the template crystallographic structure of the major facilitator superfamily proton-xylose symporter XylE, an *Escherichia coli* homologue of GLUT-1 (PDB ID: 4GC0), based on the work of Sun et al.[31,34] Then, using UCSF Chimera, all of the ligands were removed to facilitate the preparation of MD. To have the same number of amino acids, only residues 10−455 were kept. The hydrogen atoms were added via the AddH tool of UCSF Chimera using the method considering the possible hydrogen bonds.

MD simulations were performed using Amber18 software, with the ff14SB force field at a constant pressure of 1 atm maintained with a Berendsen barostat, at a constant temperature of 300 K with a Langevin thermostat, and with periodic boundary conditions in an orthogonal box with TIP3P water and $Na^+$ counterions to neutralize the system.

The systems were minimized by 1000 steps of the steepest descent algorithm, followed by 1000 steps of the conjugate gradient algorithm with restraints on $\alpha$ carbons. Afterward, the systems were brought to the simulation temperature with a Langevin thermostat at a constant volume and restrained $\alpha$ carbons, from 0 to 300 K for 9000 steps and 300 K for another 1000 steps. Then, 2 ns equilibrium simulations were performed using the production conditions with restraints of alpha carbons to allow the correct positioning of the side chains of the protein and water molecules. The last frame of each equilibration step was used to launch three replicas of 50 ns of MD simulation for each system. An integration step of 2 fs was used, with the SHAKE algorithm constraining bonds involving hydrogen due to the use of TIP3P water, PME with a cutoff of 8 Å, and effective Born radii of 14 Å in the generalized Born approximation. Finally, the water molecules were removed, and then the frames were aligned on the position of $\alpha$ carbons of the first frame for each trajectory using cpptraj utility, before the trajectories were compared using SINAPs.

*Real-Life Application to a Drug Candidate: 28 kDa Glutathione-S-transferase.* The 28 kDa glutathione-S-transferase protein (P28GST), a schistosome enzyme, is a drug candidate with anti-inflammatory properties developed by Par'Immune for the treatment of chronic inflammatory bowel disease.[35] The biological activity combines immunogenic properties[36] with both glutathione-S-transferase (GST)[37,38] and prostaglandin D synthase (PGDS)[39] enzymatic activities. Molecular mechanisms of the enzymatic activities remain to be elucidated, in particular the involved amino acids. Up to now, only the tyrosine residue in position 10 was identified as the cornerstone of both enzymatic activities via the activation of glutathione, either into a cosubstrate of GST or into a cofactor of PGDS.[37,40] Upon glutathione activation, two conformations of Tyr10 are observed from crystallography:[40] an IN conformation, where it points toward the catalytic site and the glutathione, and an OUT conformation, where it points toward the outside of the protein and is exposed to the cellular environment (Figure 4).

To study the molecular interaction networks ruling the P28GST function and to investigate the main differences between these two conformations, three classical MD replicas of 1.5 $\mu$s each were performed, starting from a crystallographic structure in its dimeric form (PDB ID: 1OE8)[40] and modified to exhibit the Tyr10 IN conformation in one monomer and the Tyr10 OUT conformation in the other one. In addition, to overcome the defects of the crystallographic structure, the side chain of Phe38 was restored and the last four amino acids of each monomer were reconstructed using UCSF Chimera.

MD simulations were performed using Amber18 following the protocol described previously. After removing the water molecules and fitting the protein to the t0 $\alpha$ trace, the three replicas were merged as 225 000 trajectory frames. One-tenth of this trajectory was sampled and submitted as a reasonable input set to the SINAPs program. The first SINAPs analysis compared the whole trajectory against itself to study the intramolecular interaction network ruling the quaternary protein state. After separating the two monomers to generate separate sets of


https://doi.org/10.1021/acs.jcim.1c00854
J. Chem. Inf. Model. 2022, 62, 1425−1436

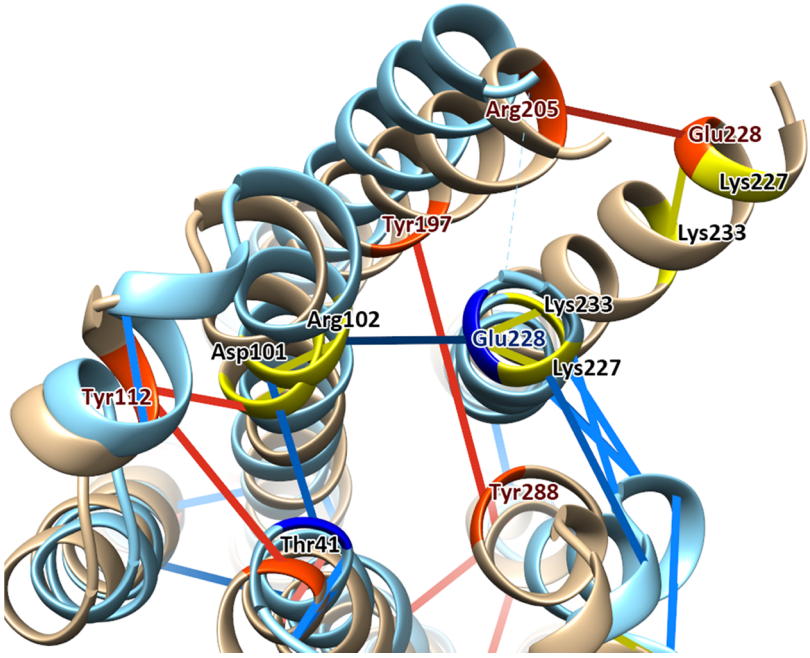


**Figure 5.** Interaction network at the cytoplasmic surface of A2AR (cyan) and A2AR* (beige) states. Common salt bridges are shown in dark yellow, whereas R* exclusive salt bridges and hydrogen bonds are displayed, respectively, in dark and light red. Exclusive R salt bridges, side chain−side chain hydrogen bonds and side chain−backbone hydrogen bonds are shown, respectively, in dark and pale blue.

trajectories, the second SINAPs analysis was related to the differential interaction network occurring in each monomer and depending on the conformational state of Tyr10.

**Applying SINAPs.** After obtaining the main input files of all of the cases under investigation, they were studied using SINAPs. Crystallographic structures of A2AR (in the PDB format) were studied by changing several parameters. To compensate for the resolution of the crystallographic structures, the hydrogen bonds and salt bridges parameters were upped by a 15% tolerance around the usual distance and angle limits. The lower limit angle taken into consideration was set at 115°, and the maximum distance was set at 4 for a hydrogen bond and 6 Å for a salt bridge.[23,24] Regarding the interactions made by ligands, only the study of hydrogen bonds is currently possible.

Trajectory files (in the nc format) and topology files (in the parm7 format) of the GLUT-1 and P28GST cases were analyzed using the default settings of the software. The hydrogen bonds and salt bridges were searched with a lower limit angle set at 135° and with the maximum distance between donor and acceptor atoms set at 3.5 and 5 Å, respectively.[23,24] Parallel pi-stackings were searched among aromatic amino acids with a distance between the centers of mass of the aromatic rings between 3 and 5 Å and a maximal planar angle set at 30°.[25,26] T-shaped and L-shaped pi-stackings were defined among aromatic amino acids with a distance between 4.5 and 7 Å.[25,26] To limit the number of interactions taken into consideration and to therefore reduce the calculation time, the minimum frequency cutoff was set at 1%. To highlight the key interactions of our case studies, the minimum frequency cutoff was set at 50% for the analysis of network interactions from MD simulations.

All of the figures presented in this article are screenshots from SINAPs' UCSF Chimera extension.

## RESULTS AND DISCUSSION

**Adenosine A2A Receptor.** *Differential Intramolecular Interactions between the A2AR Conformational States.* The first observation carried out on the crystallographic structures of A2AR was to compare the main interaction networks formed between transmembrane helices depending on the conformation (Figure 5).

An interaction network can be detected with stable salt bridges between Asp101 and Arg102, between Lys227 and Glu228, and between Glu228 and Lys233, found in all conformations. However, a salt bridge can be observed between Arg102 and Glu228 only in the inactive conformation and replaced by another salt bridge between Arg205 and Glu228 only in the active conformation, through the TM6 tilt.

A second interaction network made of hydrogen bonds was highlighted between TM6 and TM7 helices in R and R′ conformations. This network involves the Lys227, His230, Ser234, and Phe242 on TM6 and the Asn280, Arg291, and Arg293 on TM7. This network also involves interactions between TM7 and TM3/TM5 helices depending on the studied conformation. A hydrogen bond between the Tyr288 from TM7 and the Arg102 from TM3 is observed in the R′ conformation, replaced by a bond between the Tyr288 and Tyr197 from TM5 in R*.

In the literature, the amino acids described in this study are part of the structural pattern preserved in the vast majority of GPCRs. Asp101, Arg102, and Glu228 are described as part of the E/DRY motif[41] and amino acids ranging from Asp284 to Tyr288 as part of the NPxxY motif.[42]

The E/DRY motif plays a pivotal role in regulating GPCR conformational states.[41] The salt bridge between Arg102 and Glu228 is described as forming an ionic lock that stabilizes the receptor in an inactive form. This ionic lock allows the intracellular end of TM6 to be bent toward TM3 in the inactive conformation.[29,43]

In the intermediate-active conformation, Arg102 of the E/DRY motif no longer participates in the ionic lock but interacts with Tyr288 of the NPxxY motif, bringing TM3 closer to TM7.[44] TM6 is still held in place near TM7 by a network of


https://doi.org/10.1021/acs.jcim.1c00854
J. Chem. Inf. Model. 2022, 62, 1425−1436

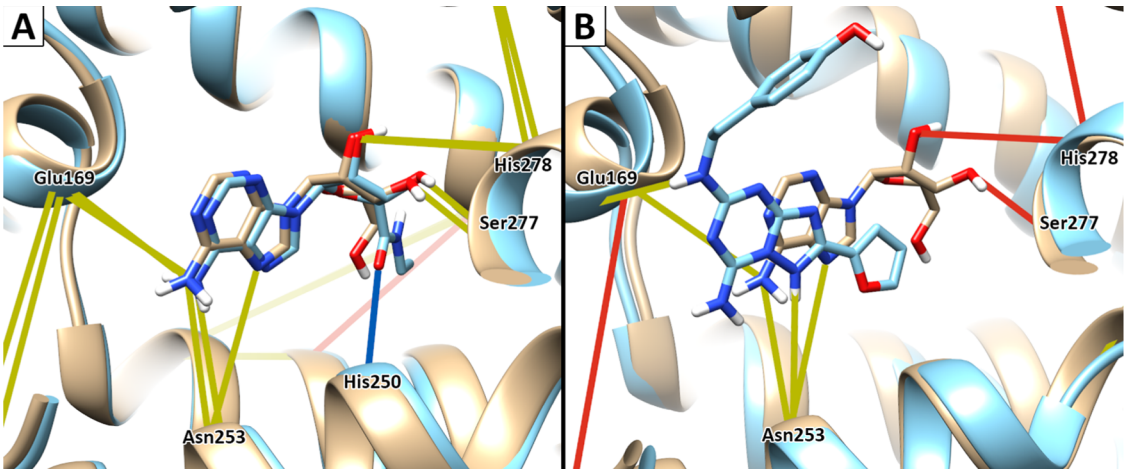


**Figure 6.** Receptor−ligand interaction networks in A2AR conformations. (A) Interaction network between adenosine and R′ (beige) and then between NECA and R* state (cyan), where common hydrogen bonds are shown in yellow, adenosine-exclusive hydrogen bonds in red, and NECA-exclusive hydrogen bonds in blue. (B) Interaction network between adenosine and the R′ state (beige) and then between ZM241385 and the R state (cyan), where common hydrogen bonds are shown in yellow, adenosine-exclusive hydrogen bonds in red, and ZM241385-exclusive hydrogen bonds in blue.

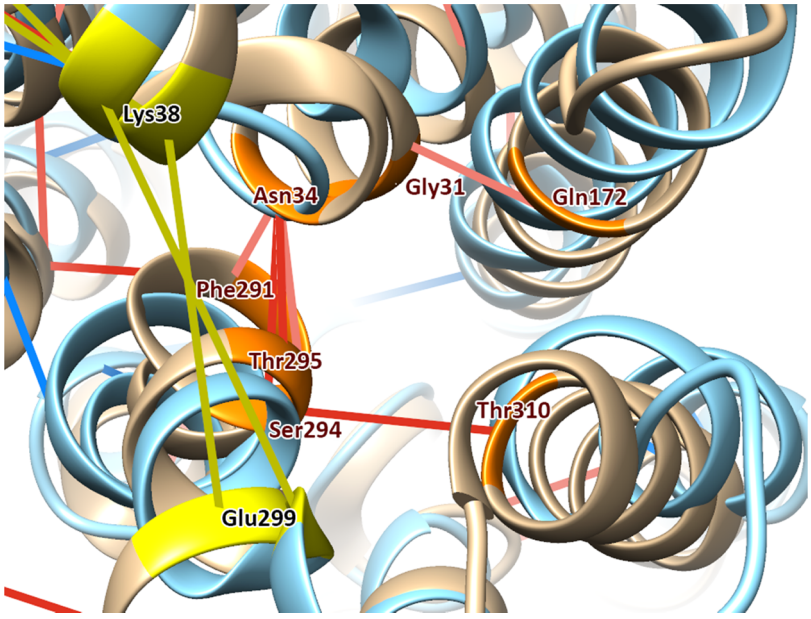


**Figure 7.** Interaction network in open (beige) and closed (cyan) EG of GLUT-1. Common salt bridges are shown in yellow, whereas exclusive hydrogen bonds between open EG amino acids are displayed in red and exclusive hydrogen bonds between closed EG are in light red.

hydrogen bonds involving residues on either side of the NPxxY motif, but it is no longer interacting with TM3 with the deflection of the ionic lock.

Finally, the interaction found only in the active conformation between Tyr288 of the NPxxY motif and Tyr197 is described as critical for forming the active state, as it operates as an activation-associated microswitch,[27,42,45] which enables the tilting of TM6 to allow a G-protein to interact.[46] Since water molecules were removed, it would be relevant to evaluate their involvement in this interaction.[44] Moreover, after tilting, TM6 is maintained against TM5 by a salt bridge between Glu228 of the E/DRY pattern with Arg205.[45]

It is also worth mentioning that other observed phenomena are not covered in depth in this paper. These include the involvement of Asp52, Ser91, and Ser281 in the formation of a dense hydrogen bond network in the intermediate-active and active conformations, supposed to be significant in the signal transduction mechanism of class-A GPCR.[47,48] Differences in hydrogen bonds network of the E/DRY motif with Ser41 and Tyr112 are also observed and may have direct implications in G-protein activation.[49]

*Differential Ligand-Binding Modes between the A2AR Conformational States.* The second observation made was to compare the binding mode of studied crystallized ligands within their active sites. The ligand of the active form, NECA, as well as that of the intermediate-active form, adenosine, spread identically into the binding site and interact by hydrogen bonds with Glu169, Asn253, Ser277, and His278. Due to the additional methylamide group of NECA, this allows an additional hydrogen bond with His250 (Figure 6A). The ligand of the inactive form, ZM241385, only binds by two hydrogen bonds with Glu169 and Asn253 (Figure 6B).



https://doi.org/10.1021/acs.jcim.1c00854
J. Chem. Inf. Model. 2022, 62, 1425−1436

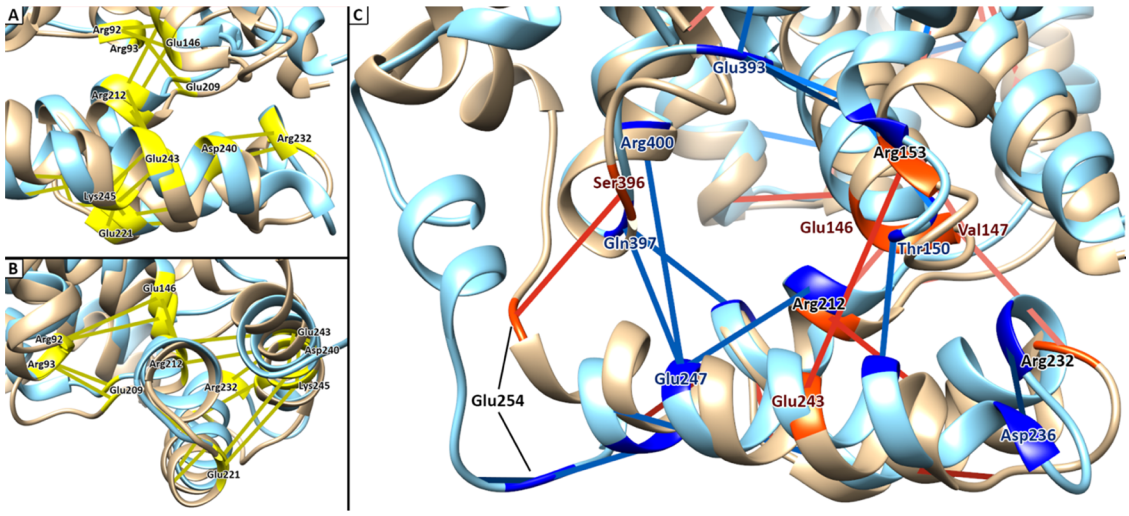


**Figure 8.** Interaction network in open (beige) and closed (cyan) IG of GLUT-1 from two orthogonal points of view (A–B). In the open IG, exclusive salt bridges are shown in dark red, exclusive side chain–side chain hydrogen bonds in red, and exclusive side chain–backbone hydrogen bonds in light red. In the closed IG, exclusive salt bridges are shown in dark blue, exclusive side chain–side chain hydrogen bonds in blue, and exclusive side chain–backbone hydrogen bonds in light blue (C).

The interactions found by SINAPs for all of these ligands are found in the literature.[50] Moreover, Ser277 and His278 are highly conserved in evolution and play a key role in the activation of the receptor,[29] and the implication of all residues mentioned above in the binding of an agonist and/or an antagonist is verified by mutational analysis.[51]

**Glucose Transporter-1.** Two aspects of the conformational changes of GLUT-1 were examined. The first one was the extracellular gate, which occludes the ligand-binding site from the extracellular environment and promotes opening to the intracellular side in the inward-open conformation. The second aspect was the intracellular gate, with a dense network of salt bridges and hydrogen bonds at the intracellular side working as a door closer.

Both examined conformations of GLUT-1 exhibit alternatively the closed extracellular ligand-binding gate (EG) with the closed intracellular gate (IG) and then the closed EG with the open IG (Figure 3).

The EG is defined by amino acids located on the extracellular ends of transmembrane helices TM1, TM5, TM7, and TM8 (Figure 7). A common salt bridge is found between Lys38 on the TM1 helix and Glu299 on the TM7 helix. A clear difference exists at the level of the interaction network between open and closed EG. In open EG, hydrogen bonds exist between Gly31 and Asn34 on the TM1 helix, Gln172 on the TM5 helix, Phe291, Ser294, and Thr295 on the TM7 helix, and Thr310 on the TM8 helix, whereas no interaction is observable in closed EG.

The IG is defined by amino acids located on the intracellular helices IC1 to IC4 and on the intracellular ends of transmembrane helices TM3, TM4, TM9, and TM10 (Figure 3). A common dense network of salt bridges is observed between Arg212, Glu221, Arg232, Asp240, Glu243, and Lys245, allowing to stabilize the IC1 to IC3 helices together. This helix bundle is then connected by other salt bridges to TM3 with the participation of Arg93 and Glu209 and to TM4 by Glu146 and Arg212. Finally, there are other notable common salt bridges between the Arg92 of TM3 and the Glu146 of TM4, between the Arg333 of TM9 and the Glu393 of TM10, and between the Arg334 of TM9 and the Glu454 of TM12 (Figure 8A,B).

Furthermore, notable differences were identified between the two studied conformations.

In the open IG conformation, the exclusive interactions bring the helices IC1 to IC3 closer to the N-domain, with a salt bridge between the Glu243 of IC3 and the Arg153 of TM4 and with two backbone–side chain hydrogen bonds, between the Arg212 of IC1 and the Glu146 of TM4, and between the Arg232 of IC2 and the Val147 of TM4. Interactions also bring the IC4 helix closer to the C-domain, with a hydrogen bond between the side chains of Ser396 of TM10 and Glu254 located on the coil before IC4. Glu254 also interacts by a backbone–backbone hydrogen bond with the Gln250 of IC3, lengthening the IC3 helix and positioning the IC4 coil in the direction of the cell membrane (Figure 8C).

In the closed IG, the exclusive interactions have the opposite effect, as they bring the helices IC1 to IC3 closer to the C-domain, with a salt bridge between the Glu247 of IC3 and the Arg400 of TM10, and two hydrogen bonds connecting the Glu247 of IC3 and the Asn217 of IC1 with the Gln397 of TM10. This helix complex is still linked to the C-domain with a hydrogen bond between the Asp240 of IC3 and the Thr150 of TM4. The two domains are also close together, with a dense interaction network between the Ser148 of TM4, the Arg153 and Gly154 of TM5, the Glu393 of TM10, and the Arg333 of TM9. Finally, the interactions between IC4 and TM10 are no longer present, as they are replaced by a strong interaction between the Arg249 of IC3 and the Glu254 located on the coil before IC4, positioning the IC4 coil in the direction of the intracellular medium (Figure 8C).

GLUT-1 has several interaction networks found to be stable and unchanged regardless of the state or evolving during the passage between the different conformations of the protein during glucose transport.

A first interaction network mainly composed of hydrogen bonds is only found at the open EG. This network allows transmembrane helices TM3, TM4, TM9, and TM10 to be brought together close to the extracellular side in the open IG. This hydrogen bond network is also described in the literature as allowing to tag the ligand-binding site in the open IG.[31,52]



https://doi.org/10.1021/acs.jcim.1c00854
J. Chem. Inf. Model. 2022, 62, 1425–1436

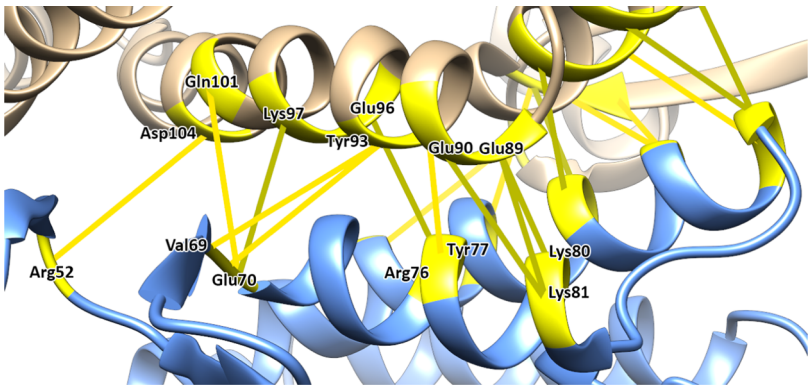


**Figure 9.** Interaction network at the dimer interface of P28GST. Common salt bridges are shown in dark yellow, and common hydrogen bonds are shown in bright yellow.

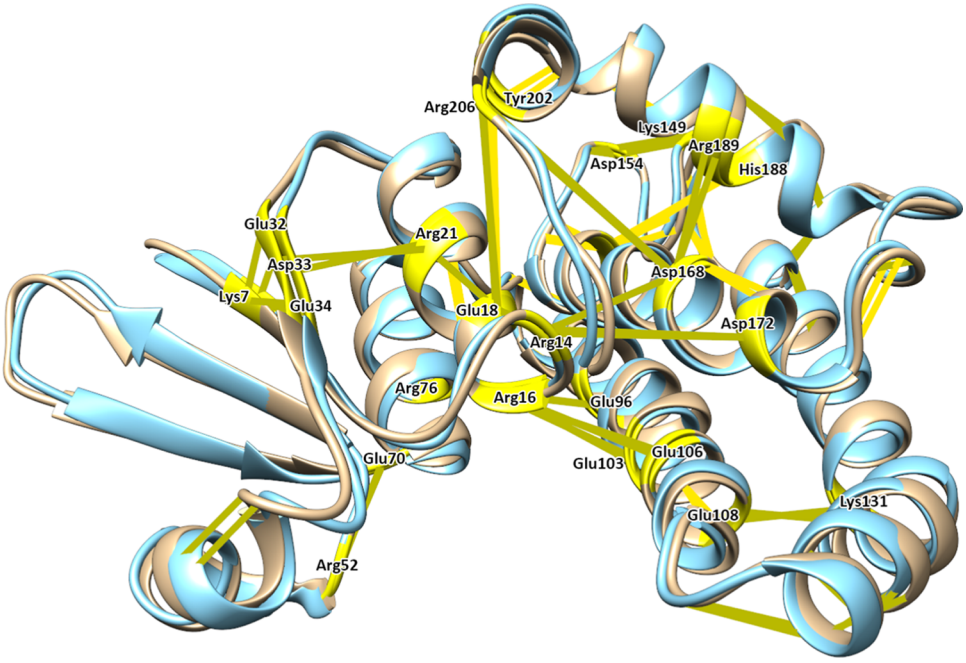


**Figure 10.** Common interaction network stabilizing the tertiary organization of P28GST. Common salt bridges are shown in dark yellow, and common hydrogen bonds are shown in bright yellow.

A second interaction network of stable salt bridges, found in the two oEG/cIG and cEG/oIG studied conformations, stabilizes helices IC1 to IC3 together, as well as these helices with the N-domain through interactions with TM3 and TM4. However, additional interactions, hydrogen bonds and salt bridges, are observed depending on the conformation of the protein, allowing varying the distance between the helices IC1 to IC3 and the C-domain, as well as the change in the geometry of the coil containing IC4. The inward-open conformation sees IC1 to IC3 helices interacting with the N-domain, when they rather interact with the C-domain in the occluded conformation. These differences are found in the literature, where all of the cited substructures form a "door closer," which restrains the opening degree of the two domains toward the intracellular side.[53,54]

However, nothing in the literature refers to the involvement of Glu254 observed in this study. Differences in its interactions can explain the variation in the positioning of the IC4 helix coil in the studied conformations. Further studies are needed to minimize the biases present in this study, to confirm the presence of these interactions and to assess the contribution of Glu254 in the change of the geometry of IC4 during glucose transfer.

Furthermore, as the E329Q mutation has not been restored, its involvement has not been measured. However, its proximity to the Gly154 and Lys155 residues allows hypothesizing the involvement of this amino acid in the dense interaction network bringing together the two domains in the occluded conformation.[31]

Despite the simplifications made in this study, it is possible to retrieve the very specific interaction networks of GLUT-1 described in the literature. From advanced MD simulations such as steered MD by simulating the passage of glucose from the extracellular to the intracellular side, it is conceivable to analyze the different conformations obtained by creating subtrajectories for each conformation and analyze them with SINAPs tools. This analysis would easily identify from a simplified tridimensional representation the major differences in the interaction networks, thus accelerating the studies conducted in the framework of a research project.



https://doi.org/10.1021/acs.jcim.1c00854
J. Chem. Inf. Model. 2022, 62, 1425−1436

**28 kDa Glutathione-S-transferase.** *Quaternary Structure of P28GST—Dimer Interface.* The quaternary organization of P28GST is based on axial symmetrical salt bridges and hydrogen bonds between dimers.

A total of six salt bridges were found between Glu70 and Lys97, Glu89 and Lys80, Glu89 and Lys81, Glu96 and Arg76, Glu90 and Lys81, and between Asp104 and Arg52. Interestingly, the four salt bridges mentioned first occurred in at least 90% of MD frames. Hydrogen bonds are also observed between Val69 and Tyr93, between Glu70 and Gln101, and between Gly90 and Tyr77 (Figure 9).

Finally, since water molecules were not considered, interactions may exist between several water molecules and the acidic amino acids Glu70, Glu96, Glu103, and Asp104, all exposed in the direction of the other monomer. The involvement of a divalent cation with its stabilizing water molecules at the dimer interface may also exist, as suggested by other proteins of the same enzyme family,[55] but this cation has not been described in the crystal structures of P28GST.

*Tertiary Structure of P28GST—Common Interactions.* The tertiary organization of P28GST is ruled by a very high number of salt bridges stabilizing the different secondary structures and coils together (Figure 10). At a frequency higher than 90%, nine salt bridges covering the whole structure are observed, with the contribution of Lys7, Glu18, Arg21, Glu32, Asp33, Glu34, Arg76, Glu96, Glu108, Lys131, Lys149, Asp154, Asp168, and Arg206. At a frequency higher than 50%, seven other salt bridges are found, with the contribution of Arg14, Arg16, Glu18, Arg52, Glu70, Glu103, Glu106, Asp168, Asp172, and Arg189. In addition, a few hydrogen bonds supplement the dense salt bridges' interaction network with the participation of Glu18, Asp160, His188, and Tyr202.

Moreover, some hydrogen bonds stabilize a coil from amino acids Ser146 to Thr157 in an unconventional shape with three turns (Figure 11). A side chain−side chain hydrogen bond is found between Asp160 and Thr157. Five backbone−side chain bonds are found between Thr157 and Asp160, Asp160 and 151, Leu150 and Ser146, Ser146 and Gly148, and between Lys149 and Asp154. Finally, two backbone−backbone hydrogen bonds are found between Leu150 and Gly153 and between Leu158 and Met84.

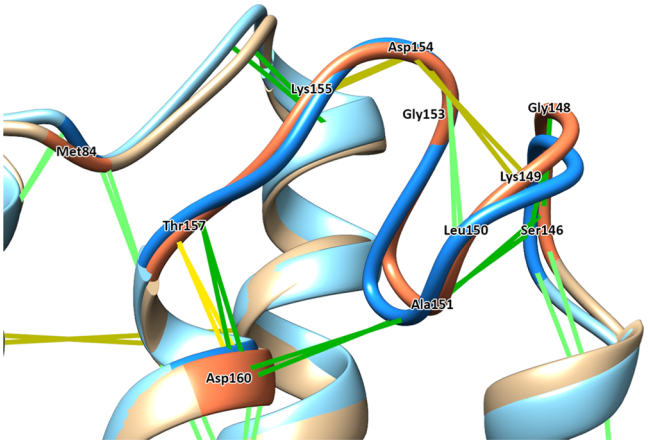


**Figure 11.** Interaction network stabilizing a coil between Ser146 and Thr157 within P28GST. Common salt bridges are shown in dark yellow, common side chain−side chain hydrogen bonds in bright yellow, common side chain−backbone hydrogen bonds in dark green, and common backbone−backbone hydrogen bonds in bright green.

*Tertiary Structure of P28GST—Tyr10 Conformation-Specific Interactions.* When comparing monomers with each other, specific interactions are highlighted, arranging the environment around Tyr10 in a different way depending on its conformation (Figure 12).

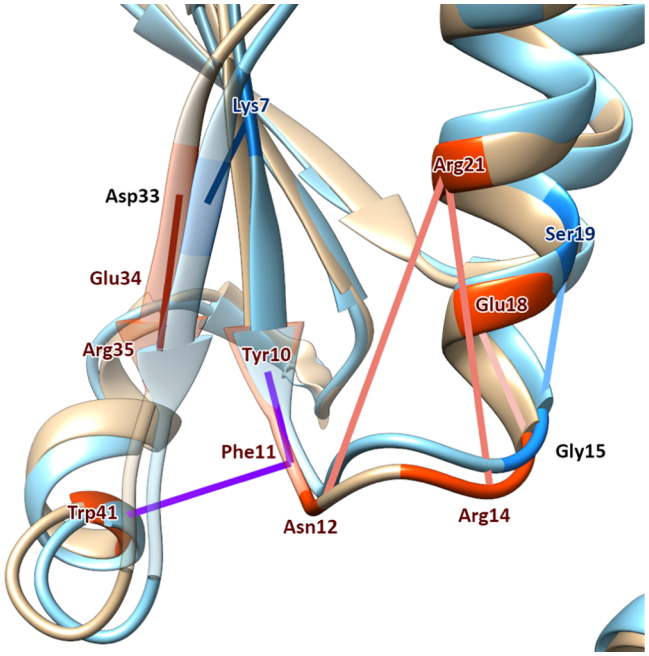


**Figure 12.** Differences in the interaction network around the catalytic Tyr10 between the IN conformation (in beige and orange) and the OUT conformation (in cyan and blue). IN exclusive salt bridges are displayed in dark red, side chain−backbone hydrogen bonds in light red, backbone hydrogen bonds in pink, and aromatic interactions in purple. OUT exclusive salt bridges are displayed in dark blue and backbone hydrogen bonds in cyan.

In the Tyr10 IN conformation, Tyr10 is stabilized by an aromatic bond with Phe11, which is stabilized by another aromatic bond with Trp41. Salt bridges hold Asp33, Glu34, and Arg35 together. Lastly, the loop following Tyr10 is maintained by hydrogen bonds between Asn12 and Arg21, Arg14 and Arg21, and between Gly15 and Glu18.

In the Tyr10 OUT conformation, due to its position and close neighbors, Tyr10 is no longer stabilized. The salt bridges maintaining the polar amino acid chunk in place are no longer present, allowing Asp33 to perform a salt bridge with Lys7. Finally, the loop is no longer held in place, and there is a backbone hydrogen bond between Gly15 and Ser19, allowing the subsequent helix-$\alpha$ to be lengthened.

*Discussion.* Numerous intramolecular and intermolecular interaction networks are found in P28GST, organizing its structure.

The quaternary structure is composed of a symmetrical interaction network, including very stable salt bridges and hydrogen bonds. These numerous interactions at the interface suggest the biological stability of P28GST as a dimer, corroborating the physical stability observable with crystallographic methods. As the SINAPs tool currently does not consider water molecules and ions, it would be worthwhile to study their impact in the formation of a hypothetical interaction network of protein−water, or protein−water−cation.



https://doi.org/10.1021/acs.jcim.1c00854
J. Chem. Inf. Model. 2022, 62, 1425−1436

The tertiary structure of P28GST is mostly supported by a dense salt bridge interaction network that holds the architecture of the protein. Further interaction networks are specific to the activation states of the protein conditioning its activity.

In the literature, no information was found on the involvement of the coil organization of amino acids Ser146 to Thr154 in proteins of the same family. In addition, no information is found when searching for specific interactions at a long range induced by the different conformations of Tyr10 down to the minimum possible frequency of 1%. The purpose of this structure, including its potential role in the mechanism of action of P28GST and in the movement of Tyr10, remains to be elucidated.

Depending on the IN or OUT conformations of Tyr10, specific interactions are found in its surroundings, governing its activation state. In the literature, site-directed mutagenesis and X-ray crystallography have highlighted the importance of the amino acids Arg21 and Arg35 in the enzymatic function of P28GST.[37]

Arg21 was identified by SINAPs as being essential for the global architecture of P28GST through salt bridges with Glu18 and Asp33. When it is mutated to leucine, thus no longer allowing the realization of salt bridges and hydrogen bonds, only the OUT conformation of Tyr10 is populated in crystallography.[37] This observation is explained by the results of SINAPs, which show the presence of specific side chain−backbone hydrogen bonds with Asn12 and Arg14 in the loop after Tyr10 in its IN conformation and thus having a possible stabilizing role of this loop.

The combined observations point to the importance of Arg21 in the motion of Tyr10 by playing a switch role, conditioning the IN and OUT conformations.

Asp33, maintained by Arg35 in the IN conformation but interacting with Lys7 in the OUT conformation, was described as a proton acceptor and could be involved in the deprotonation of Tyr10, which is then able to perform its glutathione deprotonation function after switching to its IN conformation.

Arg35, found with SINAPs to perform salt bridges with Asp33 and Glu34 only when Tyr10 is in its IN conformation, was described in the literature as performing concerted movements with the latter, allowing the formation of a ″gate″ conditioning the conformational switch of Tyr10.

Through this example, the SINAPs tool helps to find molecular interactions described in the literature within classical MD, allowing the validation of the biological reality of the simulation, and to support the hypotheses on the enzymatic mechanism of glutathione activation in P28GST. SINAPs also permits the validation of the method: as the features found here are proven by experimental evidence described in the literature, we can assume that new observations made in the future will also be valid.

## CONCLUSIONS

We presented here SINAPs, a dual analysis-visualization series of tools coded in Python, which allows a user-friendly study of the similarities and differences in nonbonded interaction networks between molecular systems. These systems may be drawn from crystallographic datasets or come from MD trajectories, thereby helping greatly in the analysis of the large amount of data generated. The visualization part is offered via an add-on to UCSF Chimera and permits a high level of user customization of the representation. Its most important advantage is to link the interactions and the structure of the proteins in a single view, while keeping the information about the type and the frequency of the interactions. It currently takes into account the intramolecular salt bridge, hydrogen bonds, and aromatic interactions as well as intermolecular hydrogen bonds, which permits to study both protein internal interaction networks throughout their conformational changes and ligand−receptor interactions, as exemplified with GLUT-1 dynamics and A2AR crystallography. The SINAPs software also enables the validation of classical MD simulations by facilitating the search for very specific interaction networks, as described here with examples from the literature, to facilitate the understanding of the mechanism of action of a target of interest and to characterize new structures, as seen with the exploratory study of P28GST.

Its integration as an easy-to-implement plugin to one of the most widely used free 3D molecular viewer opens it to both chemoinformatics experts and less experienced users from different backgrounds. This software is also scalable, with the future addition of the detection of intermolecular protein−small molecules salt bridges and aromatic interactions. Other improvements are also considered, such as hydrophobic interactions, the detection of intermolecular protein−ligand interactions in addition to the detection of hydrogen bonds already implemented, the optimization of the calculation algorithm, the current one running only on one CPU, or the improvement of the display of the results, in particular in the form of a list of interactions in UCSF Chimera, to enhance its running speed and improve the friendliness and depth of the representation.

## ASSOCIATED CONTENT

### Supporting Information

The Supporting Information is available free of charge at https://pubs.acs.org/doi/10.1021/acs.jcim.1c00854.

SINAPs_SI (in XLSX format): List of interactions observed when comparing the opened and closed intracellular gate conformations in GLUT-1 molecular dynamics simulations, within P28GST in its dimeric form, specifically at the dimeric interface of P28GST, and when comparing the IN and OUT conformations of P28GST after splitting of its monomers. The different tables, provided in different sheets, list the residue ID of acceptors and donors, the observed frequencies, and the type of bond in the specific case of hydrogen bonds (XLSX)

## AUTHOR INFORMATION


### Corresponding Authors

**Corentin Bedart** − *Univ. Lille, Inserm, CHU Lille, U1286 - Infinite - Institute for Translational Research in Inflammation, F-59000 Lille, France; Par'Immune, Bio-incubateur Eurasanté, 59120 Loos-Lez-Lille, France*; Email: c.bedart@parimmune.com

**Amaury Farce** − *Univ. Lille, Inserm, CHU Lille, U1286 - Infinite - Institute for Translational Research in Inflammation, F-59000 Lille, France*; orcid.org/0000-0003-3992-9629; Email: amaury.farce@univ-lille.fr

### Authors

**Nicolas Renault** − *Univ. Lille, Inserm, CHU Lille, U1286 - Infinite - Institute for Translational Research in Inflammation, F-59000 Lille, France*




https://doi.org/10.1021/acs.jcim.1c00854
J. Chem. Inf. Model. 2022, 62, 1425−1436

**Philippe Chavatte** − *Univ. Lille, Inserm, CHU Lille, U1286 - Infinite - Institute for Translational Research in Inflammation, F-59000 Lille, France*
**Adeline Porcherie** − *Par'Immune, Bio-incubateur Eurasanté, 59120 Loos-Lez-Lille, France*
**Abderrahim Lachgar** − *Par'Immune, Bio-incubateur Eurasanté, 59120 Loos-Lez-Lille, France*
**Monique Capron** − *Univ. Lille, Inserm, CHU Lille, U1286 - Infinite - Institute for Translational Research in Inflammation, F-59000 Lille, France; Par'Immune, Bio-incubateur Eurasanté, 59120 Loos-Lez-Lille, France*

Complete contact information is available at: https://pubs.acs.org/10.1021/acs.jcim.1c00854

### Notes

The authors declare no competing financial interest.
SINAPs is publicly available at https://github.com/ParImmune/SINAPs under a GNU General Public License v3.0. The A2AR and GLUT-1 validation datasets used to validate SINAPs are also available on GitHub. P28GST data is proprietary and thus not available.

## ■ ACKNOWLEDGMENTS

CB acknowledges a CIFRE Ph.D. fellowship from both Par'Immune (Loos, France) and the French Association Nationale de la Recherche et de la Technologie (ANRT) (CIFRE fellowship no. 2018/1313). A part of molecular dynamics simulations presented was performed using high-performance computing capabilities of Lille University data-center with the use of GPU acceleration (http://hpc.univ-lille.fr/cluster-hpc-htc).

## ■ REFERENCES

(1) Mures, O. A.; Padrón, E. J.; Raffin, B. Leveraging the Power of Big Data Tools for Large Scale Molecular Dynamics Analysis. *JP2016-XXVII Jornadas de Paralelismo* **2016**, 1−7.
(2) Bernetti, M.; Bertazzo, M.; Masetti, M. Data-Driven Molecular Dynamics: A Multifaceted Challenge. *Pharmaceuticals* **2020**, *13*, No. 253.
(3) Yu, I.; Feig, M.; Sugita, Y. High-Performance Data Analysis on the Big Trajectory Data of Cellular Scale All-Atom Molecular Dynamics Simulations. *J. Phys. Conf. Ser.* **2018**, *1036*, No. 012009.
(4) Liu, S. *Compression of Molecular Dynamics Simulation Data*; Electrical Engineering Computer Science University of California: Berkeley, 2019.
(5) Abraham, M. J.; Murtola, T.; Schulz, R.; Páll, S.; Smith, J. C.; Hess, B.; Lindahl, E. GROMACS: High Performance Molecular Simulations through Multi-Level Parallelism from Laptops to Supercomputers. *SoftwareX* **2015**, *1−2*, 19−25.
(6) Case, D. A.; Ben-Shalom, I. Y.; Brozell, S. R.; Cerutti, D. S.; Cheatham, T. E., III; Cruzeiro, V. W. D. *AMBER 2018*; University of California, San Francisco, 2018.
(7) Roe, D. R.; Cheatham, T. E. PTRAJ and CPPTRAJ: Software for Processing and Analysis of Molecular Dynamics Trajectory Data. *J. Chem. Theory Comput.* **2013**, *9*, 3084−3095.
(8) Humphrey, W.; Dalke, A.; Schulten, K. VMD: Visual Molecular Dynamics. *J. Mol. Graph.* **1996**, *14*, 33−38.
(9) Scheurer, M.; Rodenkirch, P.; Siggel, M.; Bernardi, R. C.; Schulten, K.; Tajkhorshid, E.; Rudack, T. PyContact: Rapid, Customizable, and Visual Analysis of Noncovalent Interactions in MD Simulations. *Biophys. J.* **2018**, *114*, 577−583.
(10) Contreras-Riquelme, S.; Garate, J.-A.; Perez-Acle, T.; Martin, A. J. M. RIP-MD: A Tool to Study Residue Interaction Networks in Protein Molecular Dynamics. *PeerJ* **2018**, *6*, No. e5998.
(11) Shannon, P.; Markiel, A.; Ozier, O.; Baliga, N. S.; Wang, J. T.; Ramage, D.; Amin, N.; Schwikowski, B.; Ideker, T. Cytoscape: A Software Environment for Integrated Models of Biomolecular Interaction Networks. *Genome Res.* **2003**, *13*, 2498−2504.
(12) Abdel-Azeim, S.; Chermak, E.; Vangone, A.; Oliva, R.; Cavallo, L. MDcons: Intermolecular Contact Maps as a Tool to Analyze the Interface of Protein Complexes from Molecular Dynamics Trajectories. *BMC Bioinf.* **2014**, *15*, No. S1.
(13) Mercadante, D.; Gräter, F.; Daday, C. CONAN: A Tool to Decode Dynamical Information from Molecular Interaction Maps. *Biophys. J.* **2018**, *114*, 1267−1273.
(14) Blau, C.; Grubmuller, H. G_contacts: Fast Contact Search in Bio-Molecular Ensemble Data. *Comput. Phys. Commun.* **2013**, *184*, 2856−2859.
(15) Chakrabarty, B.; Parekh, N. NAPS: Network Analysis of Protein Structures. *Nucleic Acids Res.* **2016**, *44*, W375−W382.
(16) Pettersen, E. F.; Goddard, T. D.; Huang, C. C.; Couch, G. S.; Greenblatt, D. M.; Meng, E. C.; Ferrin, T. E. UCSF Chimera - A Visualization System for Exploratory Research and Analysis. *J. Comput. Chem.* **2004**, *25*, 1605−1612.
(17) Schrödinger, L. L. C. *The PyMOL Molecular Graphics System*, Version 1.8. 2015.
(18) Laskowski, R. A.; Swindells, M. B. LigPlot+: Multiple Ligand−Protein Interaction Diagrams for Drug Discovery. *J. Chem. Inf. Model.* **2011**, *51*, 2778−2786.
(19) Morris, J. H.; Huang, C. C.; Babbitt, P. C.; Ferrin, T. E. StructureViz: Linking Cytoscape and UCSF Chimera. *Bioinformatics* **2007**, *23*, 2345−2347.
(20) Brysbaert, G.; Mauri, T.; Lensink, M. F. Comparing Protein Structures with RINspector Automation in Cytoscape. *F1000Research* **2018**, *7*, No. 563.
(21) Cock, P. J. A.; Antao, T.; Chang, J. T.; Chapman, B. A.; Cox, C. J.; Dalke, A.; Friedberg, I.; Hamelryck, T.; Kauff, F.; Wilczynski, B.; de Hoon, M. J. L. Biopython: Freely Available Python Tools for Computational Molecular Biology and Bioinformatics. *Bioinformatics* **2009**, *25*, 1422−1423.
(22) Nguyen, H.; Roe, D. R.; Swails, J.; Case, D. A. *PYTRAJ: Interactive Data Analysis for Molecular Dynamics Simulations*; Rutgers University: New Brunswick, NJ, 2016.
(23) Sticke, D. F.; Presta, L. G.; Dill, K. A.; Rose, G. D. Hydrogen Bonding in Globular Proteins. *J. Mol. Biol.* **1992**, *226*, 1143−1159.
(24) Kumar, S.; Nussinov, R. Relationship between Ion Pair Geometries and Electrostatic Strengths in Proteins. *Biophys. J.* **2002**, *83*, 1595−1612.
(25) Banerjee, A.; Saha, A.; Saha, B. K. Understanding the Behavior of $\pi-\pi$ Interactions in Crystal Structures in Light of Geometry Corrected Statistical Analysis: Similarities and Differences with the Theoretical Models. *Cryst. Growth Des.* **2019**, *19*, 2245−2252.
(26) Lanzarotti, E.; Biekofsky, R. R.; Estrin, D. A.; Marti, M. A.; Turjanski, A. G. Aromatic−Aromatic Interactions in Proteins: Beyond the Dimer. *J. Chem. Inf. Model.* **2011**, *51*, 1623−1633.
(27) Weis, W. I.; Kobilka, B. K. The Molecular Basis of G Protein−Coupled Receptor Activation. *Annu. Rev. Biochem.* **2018**, *87*, 897−919.
(28) Doré, A. S.; Robertson, N.; Errey, J. C.; Ng, I.; Hollenstein, K.; Tehan, B.; Hurrell, E.; Bennett, K.; Congreve, M.; Magnani, F.; Tate, C. G.; Weir, M.; Marshall, F. H. Structure of the Adenosine A2A Receptor in Complex with ZM241385 and the Xanthines XAC and Caffeine. *Structure* **2011**, *19*, 1283−1293.
(29) Lebon, G.; Warne, T.; Edwards, P. C.; Bennett, K.; Langmead, C. J.; Leslie, A. G. W.; Tate, C. G. Agonist-Bound Adenosine A2A Receptor Structures Reveal Common Features of GPCR Activation. *Nature* **2011**, *474*, 521−525.
(30) Cheng, R. K. Y.; Segala, E.; Robertson, N.; Deflorian, F.; Doré, A. S.; Errey, J. C.; Fiez-Vandal, C.; Marshall, F. H.; Cooke, R. M. Structures of Human A 1 and A 2A Adenosine Receptors with Xanthines Reveal Determinants of Selectivity. *Structure* **2017**, *25*, 1275−1285.e4.

(31) Deng, D.; Xu, C.; Sun, P.; Wu, J.; Yan, C.; Hu, M.; Yan, N. Crystal Structure of the Human Glucose Transporter GLUT1. *Nature* **2014**, *510*, 121−125.
(32) Arnold, K.; Bordoli, L.; Kopp, J.; Schwede, T. The SWISS-MODEL Workspace: A Web-Based Environment for Protein Structure Homology Modelling. *Bioinformatics* **2006**, *22*, 195−201.
(33) Studer, G.; Tauriello, G.; Bienert, S.; Biasini, M.; Johner, N.; Schwede, T. ProMod3—A Versatile Homology Modelling Toolbox. *PLOS Comput. Biol.* **2021**, *17*, No. e1008667.
(34) Sun, L.; Zeng, X.; Yan, C.; Sun, X.; Gong, X.; Rao, Y.; Yan, N. Crystal Structure of a Bacterial Homologue of Glucose Transporters GLUT1−4. *Nature* **2012**, *490*, 361−366.
(35) Capron, M.; Béghin, L.; Leclercq, C.; Labreuche, J.; Dendooven, A.; Standaert, A.; Delbeke, M.; Porcherie, A.; Nachury, M.; Boruchowicz, A.; Dupas, J.-L.; Fumery, M.; Paupard, T.; Catteau, S.; Deplanque, D.; Colombel, J.-F.; Desreumaux, P. Safety of P28GST, a Protein Derived from a Schistosome Helminth Parasite, in Patients with Crohn's Disease: A Pilot Study (ACROHNEM). *J. Clin. Med.* **2019**, *9*, No. 41.
(36) Driss, V.; El Nady, M.; Delbeke, M.; Rousseaux, C.; Dubuquoy, C.; Sarazin, A.; Gatault, S.; Dendooven, A.; Riveau, G.; Colombel, J. F.; Desreumaux, P.; Dubuquoy, L.; Capron, M. The Schistosome Glutathione S-Transferase P28GST, a Unique Helminth Protein, Prevents Intestinal Inflammation in Experimental Colitis through a Th2-Type Response with Mucosal Eosinophils. *Mucosal Immunol.* **2016**, *9*, 322−335.
(37) Baiocco, P.; Gourlay, L. J.; Angelucci, F.; Fontaine, J.; Hervé, M.; Miele, A. E.; Trottein, F.; Brunori, M.; Bellelli, A. Probing the Mechanism of GSH Activation in Schistosoma Haematobium Glutathione-S-Transferase by Site-Directed Mutagenesis and X-Ray Crystallography. *J. Mol. Biol.* **2006**, *360*, 678−689.
(38) Sarazin, A.; Dendooven, A.; Delbeke, M.; Gatault, S.; Pagny, A.; Standaert, A.; Rousseaux, C.; Desreumaux, P.; Dubuquoy, L.; Capron, M. Treatment with P28GST, a Schistosome-Derived Enzyme, after Acute Colitis Induction in Mice: Decrease of Intestinal Inflammation Associated with a down Regulation of Th1/Th17 Responses. *PLoS One* **2018**, *13*, No. e0209681.
(39) Hervé, M.; Angeli, V.; Pinzar, E.; Wintjens, R.; Faveeuw, C.; Narumiya, S.; Capron, A.; Urade, Y.; Capron, M.; Riveau, G.; Trottein, F. Pivotal Roles of the Parasite PGD2 Synthase and of the Host D Prostanoid Receptor 1 in Schistosome Immune Evasion. *Eur. J. Immunol.* **2003**, *33*, 2764−2772.
(40) Johnson, K. A.; Angelucci, F.; Bellelli, A.; Hervé, M.; Fontaine, J.; Tsernoglou, D.; Capron, A.; Trottein, F.; Brunori, M. Crystal Structure of the 28 KDa Glutathione S-Transferase from Schistosoma Haematobium. *Biochemistry* **2003**, *42*, 10084−10094.
(41) Rovati, G. E.; Capra, V.; Neubig, R. R. The Highly Conserved DRY Motif of Class A G Protein-Coupled Receptors: Beyond the Ground State. *Mol. Pharmacol.* **2007**, *71*, 959−964.
(42) Katritch, V.; Cherezov, V.; Stevens, R. C. Structure-Function of the G Protein−Coupled Receptor Superfamily. *Annu. Rev. Pharmacol. Toxicol.* **2013**, *53*, 531−556.
(43) Latorraca, N. R.; Venkatakrishnan, A. J.; Dror, R. O. GPCR Dynamics: Structures in Motion. *Chem. Rev.* **2017**, *117*, 139−155.
(44) Bruzzese, A.; Dalton, J. A. R.; Giraldo, J. Insights into Adenosine A2A Receptor Activation through Cooperative Modulation of Agonist and Allosteric Lipid Interactions. *PLOS Comput. Biol.* **2020**, *16*, No. e1007818.
(45) Rosenbaum, D. M.; Rasmussen, S. G. F.; Kobilka, B. K. The Structure and Function of G-Protein-Coupled Receptors. *Nature* **2009**, *459*, 356−363.
(46) Millar, R. P.; Newton, C. L. The Year In G Protein-Coupled Receptor Research. *Mol. Endocrinol.* **2010**, *24*, 261−274.
(47) Zhang, X. C.; Cao, C.; Zhou, Y.; Zhao, Y. Proton Transfer-Mediated GPCR Activation. *Protein Cell* **2015**, *6*, 12−17.
(48) White, K. L.; Eddy, M. T.; Gao, Z.-G.; Han, G. W.; Lian, T.; Deary, A.; Patel, N.; Jacobson, K. A.; Katritch, V.; Stevens, R. C. Structural Connection between Activation Microswitch and Allosteric Sodium Site in GPCR Signaling. *Structure* **2018**, *26*, 259−269.e5.
(49) Jaakola, V.-P.; Griffith, M. T.; Hanson, M. A.; Cherezov, V.; Chien, E. Y. T.; Lane, J. R.; IJzerman, A. P.; Stevens, R. C. The 2.6 Angstrom Crystal Structure of a Human A2A Adenosine Receptor Bound to an Antagonist. *Science* **2008**, *322*, 1211−1217.
(50) Carpenter, B.; Lebon, G. Human Adenosine A2A Receptor: Molecular Mechanism of Ligand Binding and Activation. *Front. Pharmacol.* **2017**, *8*, No. 898.
(51) Kim, S.-K.; Gao, Z.-G.; Van Rompaey, P.; Gross, A. S.; Chen, A.; Van Calenbergh, S.; Jacobson, K. A. Modeling the Adenosine Receptors: Comparison of the Binding Domains of $A_{2A}$ Agonists and Antagonists. *J. Med. Chem.* **2003**, *46*, 4847−4859.
(52) Chen, L. Y.; Phelix, C. F. Extracellular Gating of Glucose Transport through GLUT 1. *Biochem. Biophys. Res. Commun.* **2019**, *511*, 573−578.
(53) Deng, D.; Sun, P.; Yan, C.; Ke, M.; Jiang, X.; Xiong, L.; Ren, W.; Hirata, K.; Yamamoto, M.; Fan, S.; Yan, N. Molecular Basis of Ligand Recognition and Transport by Glucose Transporters. *Nature* **2015**, *526*, 391−396.
(54) Galochkina, T.; Ng Fuk Chong, M.; Challali, L.; Abbar, S.; Etchebest, C. New Insights into GluT1 Mechanics during Glucose Transfer. *Sci. Rep.* **2019**, *9*, No. 998.
(55) Seo, M.-J.; Oh, D.-K. Prostaglandin Synthases: Molecular Characterization and Involvement in Prostaglandin Biosynthesis. *Prog. Lipid Res.* **2017**, *66*, 50−68.


https://doi.org/10.1021/acs.jcim.1c00854
J. Chem. Inf. Model. 2022, 62, 1425−1436